ACS APPLIED MATERIALS & INTERFACES

Research Article

www.acsami.org

Identification of Multifunctional Graphene–Gold Nanocomposite for Environment-Friendly Enriching, Separating, and Detecting Hg^{2+} Simultaneously

Zhengquan Yan,[†,‡] Hongtao Xue,[‡] Karsten Berning,[§] Yun-Wah Lam,[§] and Chun-Sing Lee*[,‡]

[†]Anhui Provincial Laboratory of Biomimetic Sensor and Detecting Technology and Solar Photovoltaic Materials Research Center, West Anhui University, Lu'an 237012, China

[‡]Center of Super-Diamond and Advanced Films (COSDAF) and Dept. of Phys. and Mater. Sci., [§]Dept. of Biology and Chemistry, City University of Hong Kong, Hong Kong, China

Supporting Information

ABSTRACT: By virtue of the specific amalgam of mercury with gold and high specific area of a graphene scaffold, an environment-friendly multifunctional graphene–gold nanocomposite (G-AuNPs) has been identified and prepared by a simple one-pot redox reaction. The resultant G-AuNPs can reversibly enrich about 94% of Hg^{2+} in water samples, which can be further separated by only a simple filtration. Importantly, the color of the G-AuNPs suspension exclusively changes from purple–red to light brown upon the addition of Hg^{2+} in the presence of ascorbic acid, which can be applied for colorimetric detection of Hg^{2+} with a detection limit (3σ, $n = 20$) of 1.6×10^{-8} mol·L^{-1}. Furthermore, using ascorbic acid as reducing agents, both the preparation process and the resultant nanocomposite are nontoxic. To the best of our knowledge, this is the first report to enrich, separate and detect Hg^{2+} contaminant simultaneously without causing any secondary pollution.

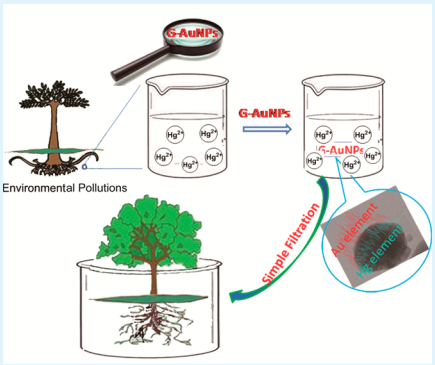

KEYWORDS: *graphene–Au nanocomposite, environment-friendly, Hg^{2+}, enrichment and separation, colorimetric detection*

1. INTRODUCTION

Fast and convenient enrichment, separation, and detection of aqueous contaminants are getting more and more important for human health and environmental protection today. Among all the environmental contaminations, heavy metal ions such as Hg^{2+} is one of the most toxic and dangerous because of its strong affinity to S-containing ligands, which blocks the sulphydryl groups (−SH) in proteins and enzymes.[1−4] Furthermore, Hg^{2+} is not biodegradable and would accumulate in animal and human bodies, which causes dysfunction of cells and results in a wide variety of diseases in the brain, kidney, central nervous system, etc.[5−8] In recent years, different approaches have been developed for Hg^{2+} detection[9−12] or separation to meet the concentration limits defined by the World Health Organization (WHO) in drinking water.[13] However, the existing literature reports are most limited to detect or separate Hg^{2+} alone. Some sensing materials applied for detecting Hg^{2+} are difficult to be separated from the test sample and so lead to seriously secondary pollutions. Therefore, there is a growing need for rapid on-site analyses using nontoxic chemosensors capable to enrich, separate, and detect Hg^{2+} contaminant simultaneously without causing a secondary pollution.[14]

Recently, gold nanoparticles (AuNPs) have attracted considerable attention in colorimetric detection of Hg^{2+}.[15−17] For example, based on the antiaggregation of AuNPs, Li et al.[18] developed a colorimetric probe for real-time detection of Hg^{2+} in water with a detection limit as low as 3.0 ppb. Owing to the fact that AuNPs surface exhibits a strong affinity for mercury, mercury will deposit on the surface of Au NPs and form a solid amalgam-like structure, which greatly influences the surface plasmonic resonance, the conjugation feature and the resultant colloid stability. For example, Using Tween 20-modified AuNPs, Lin et al.[19] reported a method to determinate Hg^{2+} by means of the formation of Hg–Au alloys on the surface of the AuNPs in the presence of citrate ions. In the presence of nontoxic ascorbic acid, Jin et al.[20] developed an eco-friendly Hg^{2+} detection method by the formation of the amalgamation between Hg and Au, which resulted in the surface plasmon resonance wavelength of AuNPs shift from long to short wavelengths with an excellent selectivity and good sensitivity for Hg^{2+} detection. Ojea-Jimenez et al.[21] found that as single entities, AuNPs could be employed for rapid sequestration of Hg^{2+} from multicomponent aqueous solutions containing low pollutant concentrations. The action mechanism was also attributed to the formation of Hg–Au alloys on the surface of AuNPs in the presence of citrate sodium as the reducing agent.

Received: October 9, 2014
Accepted: December 2, 2014
Published: December 2, 2014

Since its discovery in 2004,[22] graphene has been considered an extremely versatile sensing platform owing to its unique two-dimensional honeycomb structure, high specific area, and superior electrical conductivity. Composites from graphene and AuNPs (G-AuNPs) have been used for Hg^{2+} detection by measuring their redox potentials,[23−25] fluorescent spectra,[26,27] and surface-enhanced Ramman scattering methods[28] with excellent sensitivity and selectivity. However, there is no report on colorimetric detection of Hg^{2+} so far, let alone its application in enriching and separating Hg^{2+}. Herein, an environment-friendly multifunctional G-AuNPs has been identified and prepared for simply "naked-eye" detecting, enriching, and separating Hg^{2+} from the polluted water. The resultant G-AuNPs are expected to possess high selectivity to Hg^{2+} due to its formation of amalgam with gold,[21,29,30] excellent sensitivity by virtue of the high specific area of the graphene scaffold and a "molecular wire effect" from the synergistic interaction between graphene's π-conjugated backbone and the d-orbital of AuNPs.[31] Considering the price of gold, the sensor−Hg assembly will be easily removed from the tested samples and the sensing G-AuNPs could be regenerated simultaneously via simple filtration. To the best of our knowledge, this is the first report to enrich, separate, and detect Hg^{2+} contaminant simultaneously without secondary pollutions.

2. EXPERIMENTAL SECTION

2.1. Materials and Measurements. Mercury(II) chloride, ascorbic acid, and gold(III) chloride trihydrate were purchased from Sigma-Aldrich and all the other chemicals were of analytical reagent grade and purchased from Shanghai Chemical Reagent Company. All the reagents were used directly as received without any further purification. Water used throughout was doubly deionized.

Phosphate buffers were prepared by mixing 0.01 mol·L^{-1} H_3PO_4 solution, 0.01 mol·L^{-1} K_2HPO_4 solution, 0.01 mol·L^{-1} KH_2PO_4 solution, or 0.01 mol·L^{-1} KOH solution in a proper ratio to acquire the desired pH (pH = 3.0, 3.5, 4.0, 4.5, 5.0, 6.0, 7.0, 8.0, 9.0, 10.0).

As-prepared G-AuNPs were characterized with transmission electron microscopy (TEM) using a JEOL JEM-2100F TEM (all operated at 200 kV). Energy dispersive spectroscopy (EDS) data were acquired using TEM. Raman measurements were conducted with a Renishaw 2000 laser Raman microscope equipped with a 514 nm argon ion laser of 2 mm spot size for excitation. Concentrations of metal elements (Hg, Zn, Co, Cd, Fe and Cu) were determined using an Inductively Coupled Plasma Mass Spectrometer (ICPMS) (PerkinElmer, Elan DRC Plus). Absorption spectra were recorded with a Lambda-750 UV−is-NIR spectrophotometer.

2.2. Preparation of G-AuNPs. Graphene oxide (GO) dispersion was prepared using the method developed by Marcano et al.[32] Under the optimized condition, 100 mL 1.0×10^{-2} mol·L^{-1} $HAuCl_4$ solution was then added into 100 mL 2.0 mg/mL GO dispersion and the mixture was stirred for 2 h at room temperature. A freshly prepared ascorbic acid aqueous solution was then added dropwise into the mixture and stirred for another 2 h in an ice−water bath to reduce $AuCl_4^-$ to AuNPs. The mixture was further heated at 80 °C for 8 h. After cooling to room temperature, the dispersion was centrifuged, washed with deionized water thoroughly, and dried in an oven at 60 °C overnight.

2.3. Growth and Maintenance of Cell Culture. Human small cell lung cancinoma cell line H1299 (ATCC number CRL-580), mouse fibroblasts NIH3T3 (ATCC number CRL-1658), human alveolar type-II (ATII)-like cell lines A549 (ATCC number CCL-185), and human hepatocellular liver carcinoma cell line HepG2 (ATCC number HB-8065) were maintained in DMEM (Invitrogen, 11960-044) containing 10% fetal bovine serum (FBS) (Invitrogen, 12483-020), 1% antibiotic-antimycotic (Invitrogen 15240-062), and 1% GlutaMAX (Invitrogen, 35050-061). Cells were maintained under the standard condition (37 °C, 5% CO_2, 95% humidity).

2.4. Cytotoxicity Analysis. Cytotoxicity was evaluated by 3-(4,5-dimethyl-2- thiazolyl)-2,5-diphenyl-2H-tetrazolium bromide (MTT) assay (MTT 5 mg/mL in PBS). Cells were seeded into 96-well microculture plates at the (6×10^4 cells/mL, 100 μL/well in complete culture medium) for 24 h. Subsequently, the medium was replaced by solutions (100 μL/well) containing various concentrations of graphene gold nanoparticles (G-AuNPs) ranging from 0 to 25 μg/mL for 48 h. After 48 h of incubation, solutions containing G-AuNP were removed and 100 μL/well DMEM medium with 10% MTT stock solution were added to each well, followed by 1 h incubation. The mixture was removed and replaced by 100 μL DMSO per well, followed by another 60 min incubation at room temperature. A microplate reader (BioTek, Power Wave XS) was used to determine the absorbance at 570 nm. The estimation is based on one experiment with comprising four replicates per concentration level.

2.5. Hg^{2+} Detection Procedure. For Hg^{2+} determination, 1.0 mL phosphate buffer (pH 4.0), 1.0 mL 10 μg/mL G-AuNPs aqueous solution and 1.0 mL of Hg^{2+} solution with different concentrations were transferred into a 10 mL volumetric flask. The mixture was stirred thoroughly and finally diluted to 10 mL with doubly deionized water. After 1.0 min, the absorption spectra were measured from 400 to 700 nm and the band-slit was set as 2.0 nm. The absorption intensity change (ΔA) of the system at 545 nm was used for quantitative analysis. The decreased absorption intensity of G-AuNPs was represented as $\Delta A = A_0 - A$, where A_0 and A were the absorption intensities of the systems in the absence and presence of Hg^{2+}, respectively.

3. RESULTS AND DISCUSSION

3.1. Fabrication of G-AuNPs. For the preparation of G-AuNPs, $HAuCl_4$ solution was first added into GO dispersion and stirred for 2 h at room temperature to make $AuCl_4^-$ absorbed on the surface of GO via electrostatic interaction. Then freshly prepared ascorbic acid aqueous solution was added dropwise and kept for another 2 h in an ice−water bath to reduce $AuCl_4^-$ to AuNPs only, to make the resultant AuNPs grafted onto the GO surface tightly and evenly. At last, the mixture was heated at 80 °C for 8h to reduce GO into graphene completely. After dried in an oven at 60 °C overnight, the as-prepared sample was characterized by transmission electron microscopy (TEM), Raman spectroscopy, and UV−vis absorption measurements as shown in Figure 1.

It is easy to find from Figure 1a that the resultant AuNPs with average diameters of ca. 25 nm distribute uniformly on the surface of graphene. The reason may be attributed to van der Waals force and the hybridization between the *d* orbit of Au atom and sp^2 dangling bonds, especially the defect sites of graphene sheets.[33−37] Raman spectra of the samples (Figure 1b) exhibit both G- and D-mode peaks centered at ca. 1350 and 1590 nm, respectively, which are ascribed to vibration of the sp^2-hybridized carbon atoms in a 2D hexagonal lattice with dangling bonds in disordered plane terminations. With the formation and absorption of AuNPs on the surface of the graphene sheets, Raman signals increase. Importantly, the D-mode peak is strengthened to a larger extent than that of the G-mode peak, confirming that AuNPs are immobilized onto the surface of the graphene.[38,39] For the UV−vis spectrum, there are two obvious absorption peaks at ca. 270 and 545 nm, respectively (Figure 1c). The absorption at ca. 270 nm corresponds to the $\pi \rightarrow \pi^*$ transition of aromatic C−C bonds of the graphene matrix, indicating that GO was reduced successfully to graphene.[40] The peak at 545 nm is originated from the surface plasmon of AuNPs, which is ca. 25 nm red-shifted from that of free AuNP, hinting that AuNPs are absorbed onto the surface of graphene effectively, and there is a

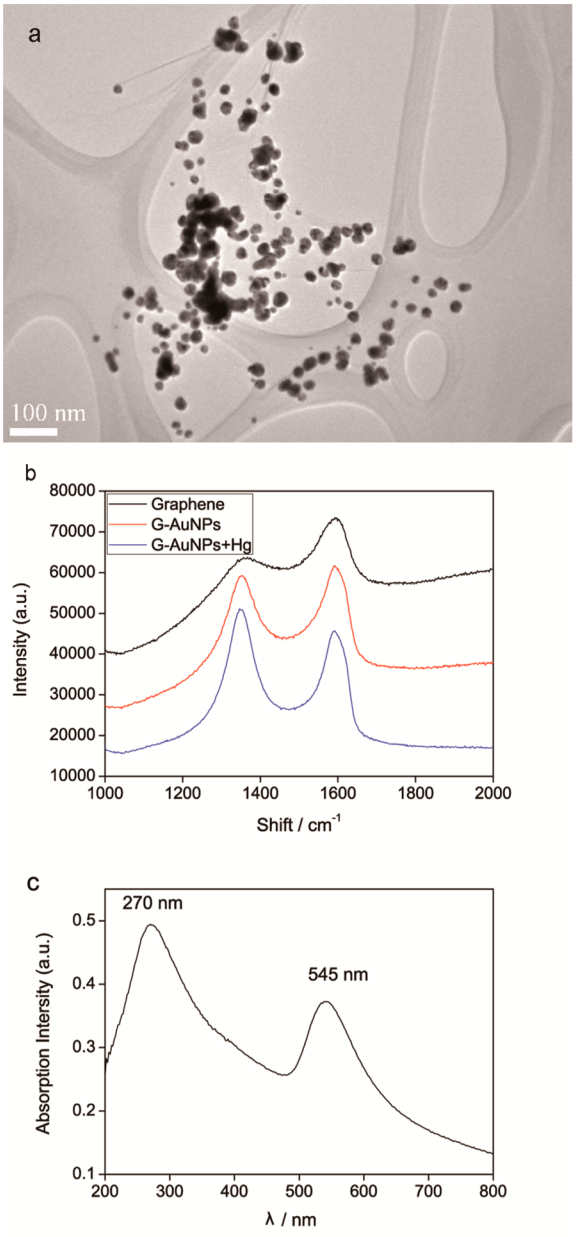

Figure 1. (a) TEM image; (b) Raman spectrum; and (c) UV−vis spectrum of the G-AuNP sample.

strong synergistic effect between AuNPs and large π-conjugated graphene matrix owing to the existence of strong $\pi-\pi$ stacking interaction and van der Waals binding.[41]

3.2. Cytotoxicity of G-AuNPs. To evaluate the cytotoxicity of G-AuNPs, a series of mammalian cell lines, namely human nonsmall cell lung carcinoma cell line H1299, human alveolar adenocarcinoma cell line A549, human hepatocellular cell line HepG2, and mouse fibroblast cell line 3T3, were incubated in the presence of increasing amounts of G-AuNPs for 48 h. After treatment, the number of viable cells was measured by the reduction of tetrazolium dye MTT, and the cytotoxicity of G-AuNPs was calculated by normalizing the MTT readings of G-AuNPs treated groups against those of the untreated control culture for the same length of time as shown in Figure 2 and Supporting Information Figure S1−3. The result shows that G-AuNPs exert a relatively low level of toxicity, as more than 50% of the cells in each cell line survived even at the highest G-

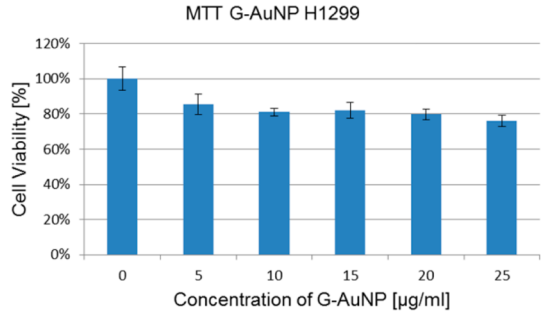

Figure 2. Cytotoxicity G-AuNPs to a series of mammalian cell lines of H1299.

AuNP concentration tested (25.0 μg/mL). Especially, for H1299 and HepG2 cells, near 80% cell viability can be still detected after they were exposed to AuNPs for more than 48 h continuously at the concentration of 25.0 μg/mL (Figure 2 and Supporting Information Figure S1). This suggests that the cytotoxicity of G-AuNPs, at concentrations relevant to its application as an Hg sensor and scavenger, is negligible to mammalian cells.

3.3. Strong Enriching Ability of G-AuNPs to Hg^{2+}. To confirm the extraction feasibility of G-AuNPs to Hg^{2+}, the amount of Hg^{2+} adsorbed on G-AuNPs was measured using inductively coupled plasma spectrometry (ICP). To do this, Hg^{2+}, Zn^{2+}, Co^{3+}, Cd^{2+}, Fe^{3+}, and Cu^{2+} ion aqueous solutions with the same concentration (1.0×10^{-5} mol·L^{-1}) were well mixed at first. The mixed metal ions solution was dropwisely added into 100 mL 25.0 μg/mL G-AuNPs dispersion in the presence of enough ascorbic acid by vigorous agitation to make the color of G-AuNPs solution change from purple−red into light brown exactly, indicating an appropriate amount of G-AuNPs and all Hg^{2+} added has been reacted into Au-amalgam. After the mixture was shaken for another 30 min and then simply filtered, all the metal ion contents remained in the resultant filtrate were measured with ICP.

As shown in Figure 3, after simple filtration, only ca. 6% Hg^{2+} remained in the resultant filtrate. This suggests that about 94%

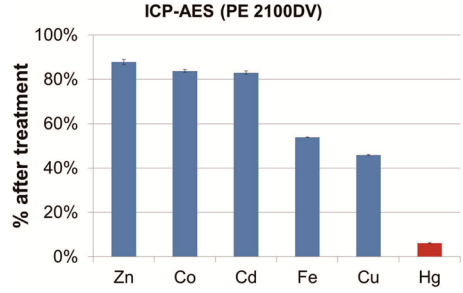

Figure 3. Residue concentrations of ions after the solution with mixed metal ions was treated with the G-AuNPs (error bars are standard deviation from five measurements).

of Hg^{2+} has been enriched and removed by the G-AuNPs composite. This shows that the G-AuNP composite is potentially useful as a stationary phase for enriching and separating Hg^{2+} in aqueous media by virtue of its high affinity to mercury. At the same time, the amount of residue for the coexisting Zn^{2+}, Co^{3+}, Cd^{2+}, Fe^{3+}, and Cu^{2+} remained in the system after reaction with G-AuNPs are ca. 88%, 84%, 83%, 54%, and 46%, respectively. These are attributed to the

dx.doi.org/10.1021/am506875t | ACS Appl. Mater. Interfaces 2014, 6, 22761−22768

nonselective physic adsorption of metal ions on the large graphene surface. Due to the higher oxidation potential of Fe^{3+} and Cu^{2+}, they might be partially reduced to neutral metal atoms by ascorbic acid and leads to increased amounts of deposition onto the graphene surface because of reduced repulsion comparing to their ions. All these results suggest that the G-AuNPs composite may be a promising adsorbent for enrichment and separation of Hg^{2+} over a range of transition and heavy metal ions.

3.4. Action Mechanism between G-AuNPs and Hg^{2+}. To experimentally illustrate the action mechanism between G-AuNPs and Hg^{2+}, TEM with energy dispersive spectroscopy (EDS) was used to study elemental and chemical compositions of the G-AuNP upon contacting with Hg^{2+} at high spatial resolution.[42,43]

Figure 4a shows a TEM image of the G-AuNP-Hg assembly after the reaction between G-AuNPs and Hg^{2+} in the presence of ascorbic acid. The corresponding EDS elemental mapping for Au (Figures 4b) and Hg (Figure 4c) show that after reacting with Hg^{2+}, G-AuNPs are composed of both Au and Hg with identically geometrical cutting edges to the TEM morphology of G-AuNPs-Hg (Figure 4a). It hints that mercury element may be absorbed onto the AuNPs efficiently. To further confirm the conclusion above, EDS line scan for Au and Hg across one of the particle was recorded as shown in Figure 4d. It is easy to see that the content of mercury is well proportionate to that of gold. All the results visually illustrate that mercury component is completely and uniformly distributed to AuNPs, and that there is little mercury absorbed on the surface of graphene. The action mechanism between G-AuNPs and Hg^{2+} was to form gold amalgam after mercury element was absorbed to AuNPs as reported before.[18,28−30]

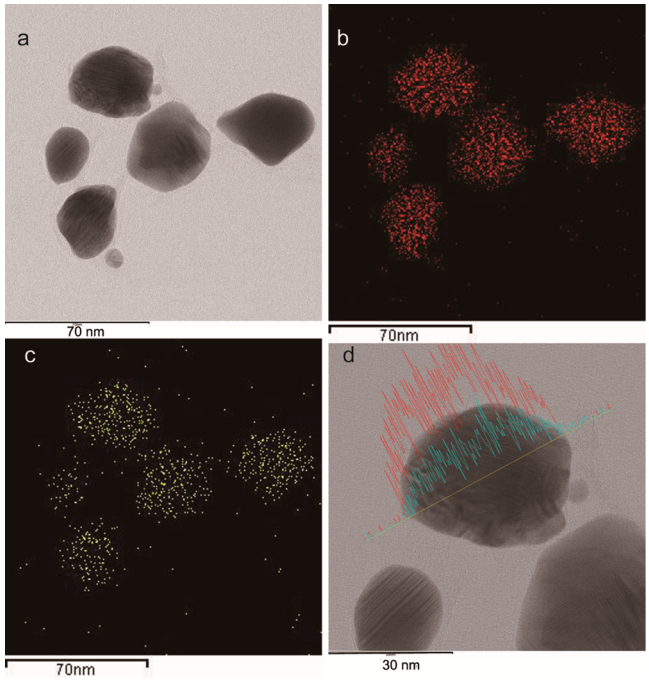

Figure 4. (a) TEM image; EDS elemental mapping of (b) Au and (c) Hg of G-AuNPs after reacting to Hg; (d) EDS line scan across one G-AuNP (red for Au and blue for Hg) in part a.

Further examination with high-resolution transmission electron microscopy (HRTEM) shows that upon forming the G-AuNPs absorbed with different contents of mercury, that is, 0, 3.26, 11.06, and 15.42 wt % mercury, respectively, defect density in the form of stacking fault increase. In the pure gold nanoparticle (Figure 5a), the fringe spacing of 0.237 nm matches well to the {111} interplanar spacing of gold. Interestingly, the lattice fringe spacing shows a corresponding increase from 0.237 to 0.249 nm as the content of Hg increases to 15.42 wt% (Figure 5d). It can considered that upon exposure to Hg^{2+} in the presence of ascorbic acid, Hg^{2+} are reduced and then diffused into the AuNPs to form highly defective gold amalgam nanoparticles.

3.5. Application for Colorimetric Detection of Hg^{2+}. *3.5.1. Optimization of Experimental Conditions.* To make sure of its practical application in colorimetric detection of Hg^{2+}, the sensing conditions of G-AuNPs were first optimized. As the redox potential between ascorbic acid and Hg^{2+} is sensitive to the pH greatly, effect of pH was investigated over pH 3.0−10.0. Figure 6 shows the changes (ΔA) in the absorption intensities at 545 nm before and after Hg^{2+} was added into G-AuNPs dispersion ($\Delta A = A_0 - A$, where A_0 and A were the absorption intensities of the systems in the absence and presence of Hg^{2+}, respectively) with different pH, that is, pH = 3.0, 3.5, 4.0, 4.5, 5.0, 6.0, 7.0, 8.0, 9.0, 10.0. It can be easily seen that pH of the solution plays an important role in the interaction between G-AuNPs and Hg^{2+}. ΔA increases gradually with the decrease of pH and reaches the maximum when pH is ca. 4.0. The reason may be that the redox potential of Hg^{2+} increases with the decrease of pH and so less Hg^{2+} can be reduced at high pH and thus lead to a weaker response. Based in Figure 6, we select a pH value of 4.0 for all subsequent tests.

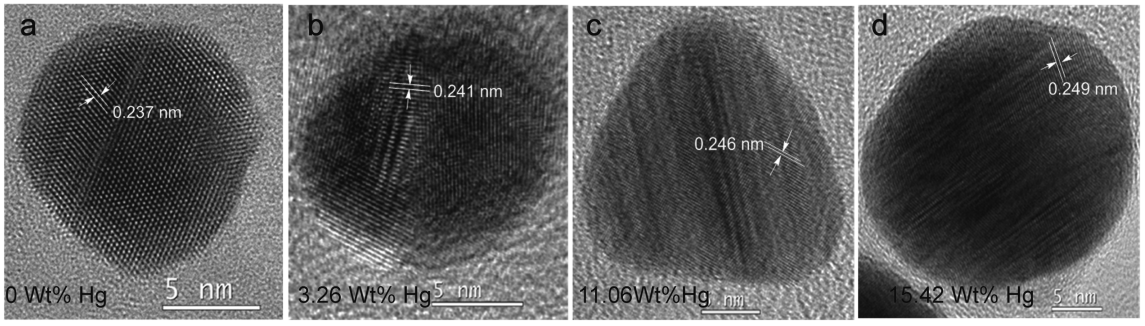

Figure 5. High-resolution transmission electron microscopy images of G-AuNPs absorbed with different contents of mercury, that is, (a) 0, (b) 3.26, (c) 11.06, and (d) 15.42 wt % mercury, respectively.

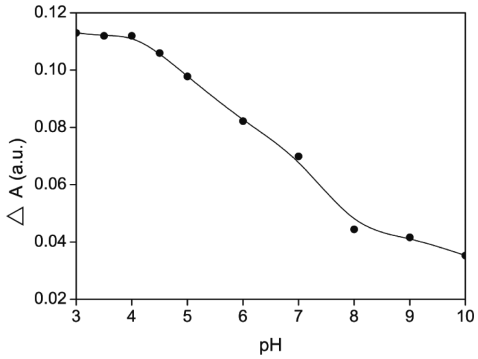

Figure 6. Effect of pH on change in absorption intensity (ΔA) of the system at 545 nm in aqueous.

To illustrate the response rate and stability of the G-AuNPs to Hg^{2+}, the absorption intensity at 545 nm of the system was measured at different times after adding Hg^{2+}. It can be seen from Figure 7 that the sensing system shows a fast response time of less than 0.5 min and stable readout in the following 1 h. We also confirmed that the absorbance at 545 nm is not influenced by the sample's ionic strength over a NaCl concentration range from 2.0×10^{-2} to 10^{-7} mol·L^{-1}, hinting that the present sensing system is reasonably stable and can be applied in various kinds of surroundings.

3.5.2. Special Selectivity to Hg^{2+}. To demonstrate the high sensitivity and selectivity of G-AuNPs to Hg^{2+}, UV−vis spectra of the system in the presence of different metal ions, that is, Fe^{3+}, Ag^{+}, Al^{3+}, Ba^{2+}, Cd^{2+}, Co^{3+}, Cu^{2+}, K^{+}, Mg^{2+}, Na^{+}, Ni^{2+}, Pb^{2+}, and Sr^{2+} all in 3.5×10^{-4} M while Hg^{2+} in only 1/100 of the other metal ions (3.5×10^{-6} M). As shown in Figure 8a, addition of these metal ions except Hg^{2+} shows negligible changes in the absorbance of the present G-AuNPs sensing system, and the changes in absorption intensity at 545 nm are all less than 5% relative to the Hg^{2+} solution with only 1/100 concentration. Importantly, the color of the G-AuNPs suspension exclusively changes from purple−red to light brown upon the addition of Hg^{2+} and little changes happened in the presence of other ions above (Figure 8b). All the results indicate that the present G-AuNPs possess an excellent selectivity for Hg^{2+} colorimetric detection.

3.5.3. Analytical Parameters and Samples Detection. Figure 9a shows the color change of G-AuNPs sensing system at different concentrations of Hg^{2+} between 0−350×10^{-8} mol·L^{-1}. From Figure 9a, it is easy to find that the color of the sensing system changes from purple−red to light brown, which can be detected by naked eye. Also, the calibration graph, the detection limit and precision for Hg^{2+} detection were obtained under the optimal conditions from Figure 9b and c. From the spectra, a calibration graph, the detection limit and precision for Hg^{2+} detection can be obtained. A linear relationship between ΔA and Hg^{2+} concentration (Figure 9c) is exhibited over the range of 0 to 350×10^{-8} mol·L^{-1} with a correlation coefficient of 0.9985. The regression equation is $\Delta A = -4.32 \times 10^{-4} + 3.30 \times 10^{-4}$ c (10^{-8} mol·L^{-1}). Based on the definition of the detection limit (LOD), three times of average deviation of absorbance at 545 nm in 20 blank samples without Hg^{2+} used here, the LOD for Hg^{2+} determination is up to 1.6×10^{-8} mol·L^{-1}, which is good enough for detecting Hg^{2+} in drinking water without sample pretreatment according to the limit of 3.0×10^{-8} mol·L^{-1} defined by the WHO.[44]

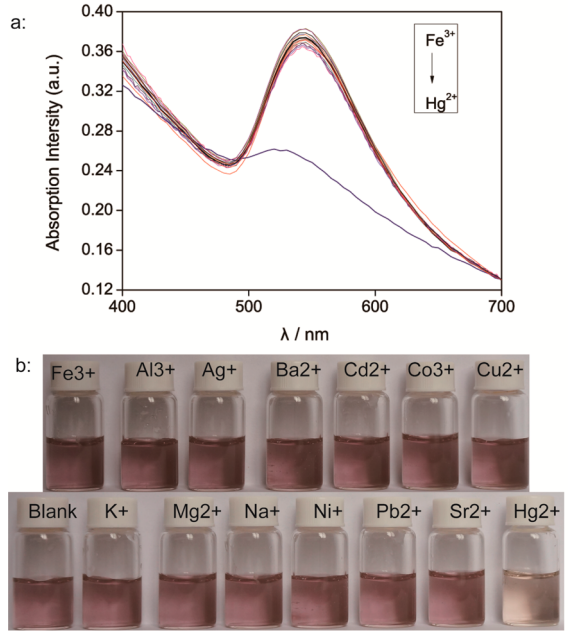

Figure 8. (a) Effects of different metal ions on the UV−vis spectra of G-AuNPs (from top to bottom: Fe^{3+}, Ag^{+}, Al^{3+}, Ba^{2+}, Cd^{2+}, Co^{3+}, Cu^{2+}, blank, K^{+}, Mg^{2+}, Na^{+}, Ni^{2+}, Pb^{2+}, Sr^{2+}, and Hg^{2+}); (b) corresponding photographs of the samples treated with different ions.

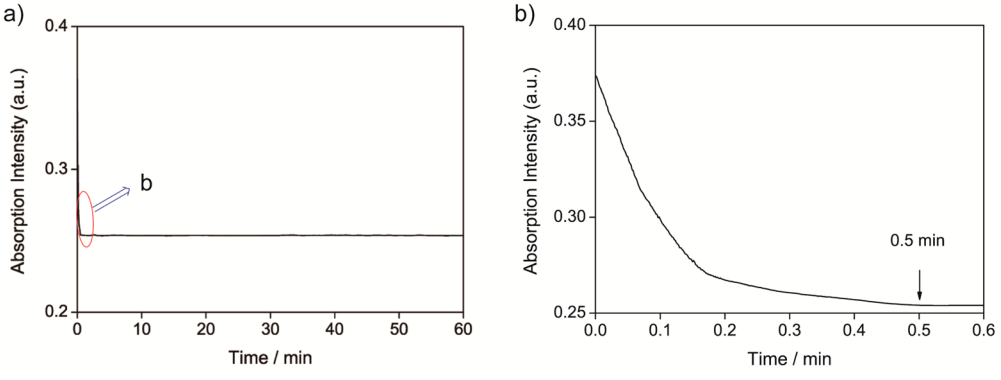

Figure 7. (a) Absorption intensity of the sensor at 545 nm upon adding Hg^{2+}. (b) The magnified curve of the response in the first 0.5 min.

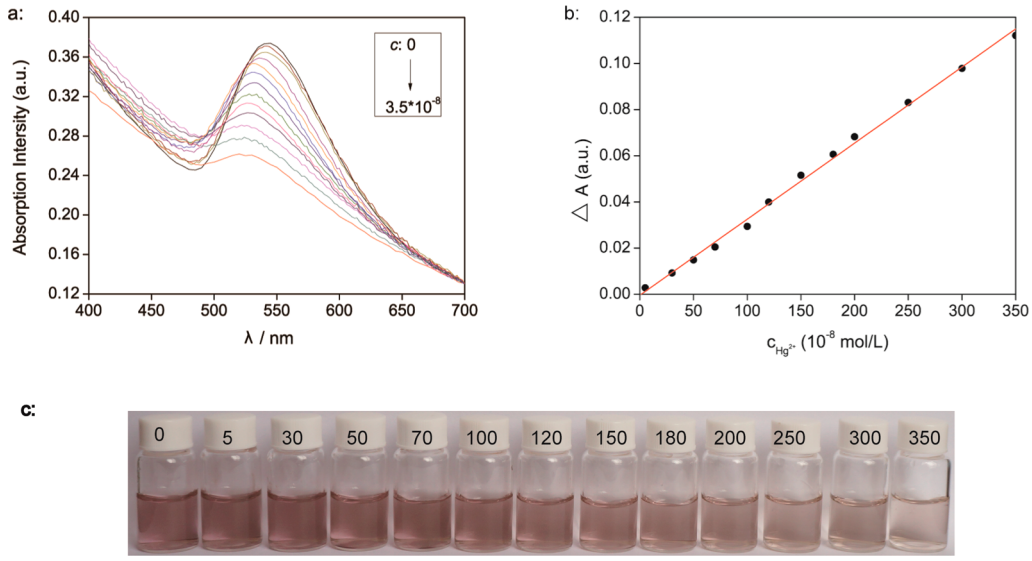

Figure 9. (a) Absorption spectra of the G-AuNP sensor system with different Hg^{2+} concentrations (from top to bottom: 0, 5.0, 30, 50, 70, 100, 120, 150, 180, 200, 250, 300, 350 × 10^{-8} mol·L^{-1}); (b) linear relationship between the Δ*A* of G-AuNPs at 545 nm and Hg^{2+} concentrations; (c) photographs of the G-AuNP sensor systems with different Hg^{2+} concentrations from 0 to 350 × 10^{-8} mol·L^{-1}.

To further demonstrate its application, the sensor was applied to determine Hg^{2+} concentrations in three environmental water samples obtained respectively from the Pi River, underground water and tap water (Table 1). All the samples were tested after filtering several times and being concentrated 100 times by evaporation. For recovery studies, a known concentration of Hg^{2+} (500 nM) was added to the environmental water samples and the total Hg^{2+} concentrations were determined with the sensor. To access the reproducibility of the method, the measurements were carried out 5 times repeatedly for each type of the environmental water. The recoveries of different known amounts of Hg^{2+} spiked were determined to be from 98.6% to 102.4% with standard deviations (RSD ≤ 2.6%). The measured Hg^{2+} concentrations in the 3 environmental water samples also agree well with our reports before using other organic colorimetric sensors.[9,11] These validate the reliability and practicality of the proposed colorimetric method for Hg^{2+} detection.

Table 1. Determination Results for Environmental Water Samples (n = 5)[a]

samples[b]	$c_{Hg^{2+}}$ in sample[b] (nM)	spiked (nM)	found (nM)	recovery (%)	RSD (%)
1 (the Pi River)	415.6	500.0	902.8	98.6	1.9
2 (underground)	866.3	500.0	1399.1	102.4	2.6
3 (tap water)	0.00	500.0	495.5	99.1	1.7

[a]Phosphate buffer, pH 4.0. [b]The environmental water Hg^{2+} concentration determined using G-AuNPs with the proposed method. The real values are the table values ×10^{-2} nmol·L^{-1} for the detected water samples were concentrated 100 times.

3.6. Reusable Property of G-AuNPs to Hg^{2+}. Considering the price of gold, the reusable property of G-AuNPs after its reaction with Hg^{2+} was studied carefully. Figure 10 shows that upon adding Hg^{2+} into the dispersion of the G-AuNP system, the color changes from purple−red to light brown. Enough EDTA was then added into the mixture under stirring thoroughly in air overnight to form colorful sediment. Due to the strong coordination action between EDTA and Hg^{2+}, the sensor is regenerated by extracting mercury from the sensor-Hg^{2+} assembly to give the colorful sediment. After filtering and washing, the colorful sediment was redispersed by sonication to regenerate the purple−red uniform suspension, which possesses the same UV−vis spectrum, as shown in Figure 1c, hinting that the regenerated G-AuNPs composite could work repeatedly.

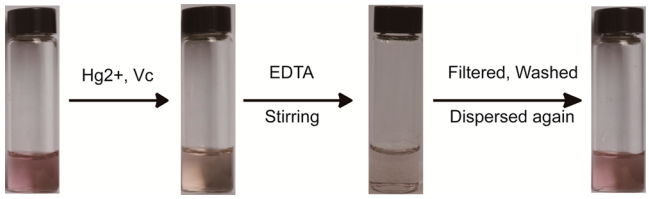

Figure 10. Color changes showing the reversibility of G-AuNPs-based sensing system.

4. CONCLUSION

An environment-friendly and nontoxic graphene−Au nanocomposite (G-AuNPs) has been designed and fabricated for colorimetric detection, enrichment, and separation of Hg^{2+} simultaneously, without any secondary pollution accompanying with color change from purple−red to light brown color. By virtue of their high affinity and superhigh specific surface area, the reaction between G-AuNPs and Hg^{2+} is to form gold amalgam. The system can enrich and separate Hg^{2+} as high as 94% in practice by a simple filtration process. As the resultant G-AuNPs are relatively nontoxic to mammalian cells, they are also applicable as a reusable colorimetric sensor for detection of Hg^{2+} in aqueous without secondary pollutions. The work will provide a generic and effective strategy to construct environment-friendly colorimetric materials for analyzing and separating species at a low concentration with a rapid-assessment process and open up ways for simply enriching and separating various biological and chemical toxic ions without sophisticated instruments.

■ ASSOCIATED CONTENT

Supporting Information

Figures of the cytotoxicity of G-AuNPs to a series of mammalian cell lines of HepG2, A549, and NIT3T3. This material is available free of charge via the Internet at http://pubs.acs.org/.

■ AUTHOR INFORMATION

Corresponding Author

*E-mail: apcslee@cityu.edu.hk.

Notes

The authors declare no competing financial interest.

■ ACKNOWLEDGMENTS

The authors gratefully acknowledge the financial supports from the City University of Hong Kong via a Strategic Research Grant (No. 7004008), National Natural Science Foundation of China (No. 21277103), and Anhui Provincial Natural Science Fund (Title: 3-D graphene-based porous composites and their applications in enrichment detection and separation of water pollution).

■ REFERENCES

(1) Kim, H. N.; Ren, W. X.; Kim, J. S.; Yoon, J. Fluorescent and Colorimetric Sensors for Detection of Lead, Cadmium, and Mercury ions. *Chem. Soc. Rev.* **2012**, *41*, 3210−3244.

(2) Fitzgerald, W. F.; Lamborg, C. H.; Hammerschmidt, C. R. Marine Biogeochemical Cycling of Mercury. *Chem. Rev.* **2007**, *107*, 641−662.

(3) Onyido, I.; Norris, A. R.; Buncel, E. Biomolecule-Mercury Interactions: Modalities of DNA Base-Mercury Binding Mechanisms. Remediation Strategies. *Chem. Rev.* **2004**, *104*, 5911−5929.

(4) Henkel, G.; Krebs, B. Metallothioneins: Zinc, Cadmium, Mercury, and Copper Thiolates and Selenolates Mimicking Protein Active Site Features—Structural Aspects and Biological Implications. *Chem. Rev.* **2004**, *104*, 801−824.

(5) Rurack, K.; Resch-Genger, U. Rigidization, Preorientation, and Electronic Decoupling—The 'Magic Triangle' for the Design of Highly Efficient Fluorescent Sensors and Switches. *Chem. Soc. Rev.* **2002**, *31*, 116−127.

(6) Hu, L.; Yan, Z. Q.; Xu, H. Y. Advances in Synthesis and Application of Near-Infrared Absorbing Squaraine Dyes. *RSC Adv.* **2013**, *3*, 7667−7676.

(7) Feng, J. J.; Huang, H.; Chen, W. J.; Chen, J. R.; Lin, H. J.; Wang, A. J. Sensitive Detection of Mercury (II) Ion Using Water-Soluble Captopril-Stabilized Fluorescent Gold Nanoparticles. *Mater. Sci. Eng., C* **2013**, *33*, 2664−2668.

(8) Du, J. J.; Jiang, L.; Shao, Q.; Liu, X. G.; Marks, R. S.; Ma, J.; Chen, X. D. Colorimetric Detection of Mercury Ions Based on Plasmonic Nanoparticles. *Small* **2013**, *9*, 1467−1481.

(9) Hu, L.; Zhang, Y. F.; Nie, L.; Xie, C. G.; Yan, Z. Q. Colorimetric Detection of Trace Hg^{2+} with Near-Infrared Absorbing Squaraine Functionalized by Dibenzo-18-Crown-6 and Its Mechanism. *Spectrochim. Acta, Part A* **2013**, *104*, 87−91.

(10) Jiang, J.; Liu, W.; Cheng, J.; Yang, L. Z.; Jiang, H.; Bai, D. C.; Liu, W. S. A Sensitive Colorimetric and Ratiometric Fluorescent Probe for Mercury Species in Aqueous Solution and Living Cells. *Chem. Commun.* **2012**, *48*, 8371−8373.

(11) Yan, Z. Q.; Hu, L.; Nie, L.; Lv, H. Preparation of 4,4′-Bis-(Carboxyl Phenylazo)-Dibenzo-18-Crown-6 Dye and Its Application on Ratiometric Colorimetric Recognition to Hg^{2+}. *Spectrochim. Acta, Part A* **2011**, *79*, 661−665.

(12) Yan, Z. Q.; Guang, S. Y.; Xu, H. Y.; Liu, X. Y. An Effective Real-Time Colorimeteric Sensor for Sensitive and Selective Detection of Cysteine under Physiological Conditions. *Analyst* **2011**, *136*, 1916−1921.

(13) Yan, Z. Q.; Yuen, M.-F.; Hu, L.; Sun, P.; Lee, C.-S. Advance for Colorimetric Detection of Hg^{2+} in Aqueous Solution. *RSC Adv.* **2014**, *4*, 8373−48388.

(14) Nazeeruddin, M. K.; Di Censo, D.; Humphry-Baker, R.; Gratzel, M. Highly Selective and Reversible Optical, Colorimetric, and Electrochemical Detection of Mercury(II) by Amphiphilic Ruthenium Complexes Anchored onto Mesoporous Oxide Films. *Adv. Funct. Mater.* **2006**, *16*, 189−194.

(15) Kang, T.; Yoo, S. M.; Yoon, I.; Lee, S.; Choo, J.; Lee, S. Y.; Kim, B. Au Nanowire-on-Film SERRS Sensor for Ultrasensitive Hg^{2+} Detection. *Chem.—Eur. J.* **2011**, *17*, 2211−2214.

(16) Wang, L.; Li, T.; Du, Y.; Chen, C. G.; Li, L.; Zhou, M.; Dong, S. J. Au NPs-Enhanced Surface Plasmon Resonance for Sensitive Detection of Mercury(II) Ions. *Biosens. Bioelectron.* **2010**, *25*, 2622−2626.

(17) Wang, C. I.; Huang, C. C.; Lin, Y. W.; Chen, W. T.; Chang, H. T. Catalytic Gold Nanoparticles for Fluorescent Detection of Mercury(II) and Lead(II) Ions. *Anal. Chim. Acta* **2012**, *745*, 124−130.

(18) Li, Y.; Wu, P.; Xu, H.; Zhang, Z. P.; Zhang, X. H. Highly Selective and Sensitive Visualizable Detection of Hg^{2+} Based on Anti-aggregation of Gold Nanoparticles. *Talanta* **2011**, *84*, 508−512.

(19) Lin, C. Y.; Yu, C. J.; Lin, Y. H.; Tseng, W. L. Colorimetric Sensing of Silver(I) and Mercury(II) Ions Based on an Assembly of Tween 20-Stabilized Gold Nanoparticles. *Anal. Chem.* **2010**, *82*, 6830−6837.

(20) Jin, L.-H.; Han, C.-S. Eco-Friendly Colorimetric Detection of Mercury (II) Ions Using Label-Free Anisotropic Nanogolds in Ascorbic Acid Solution. *Sens. Actuators, B* **2014**, *195*, 239−245.

(21) Ojea-Jimenez, I.; Lopez, X.; Arbiol, J.; Puntes, V. Citrate-Coated Gold Nanoparticles As Smart Scavengers for Mercury(II) Removal from Polluted Waters. *ACS Nano* **2012**, *6*, 2253−2260.

(22) Novoselov, K. S.; Geim, A. K.; Morozov, S. V.; Jiang, D.; Zhang, Y.; Dubonos, S. V.; Grigorieva, I. V.; Firsov, A. A. Electric Field Effect in Atomically Thin Carbon Films. *Science* **2004**, *306*, 666−669.

(23) Zhang, Y.; Zhao, H.; Wu, Z. J.; Xue, Y.; Zhang, X. F.; He, Y. J.; Li, X. J.; Yuan, Z. B. A Novel Graphene−DNA Biosensor for Selective Detection of Mercury Ions. *Biosens. Bioelectron.* **2013**, *48*, 180−187.

(24) Wei, Y.; Gao, C.; Meng, F. L.; Li, H. H.; Wang, L.; Liu, J. H.; Huang, X. J. SnO_2/Reduced Graphene Oxide Nanocomposite for the Simultaneous Electrochemical Detection of Cadmium(II), Lead(II), Copper(II), and Mercury(II): An Interesting Favorable Mutual Interference. *J. Phys. Chem. C* **2012**, *116*, 1034−1041.

(25) Zhang, T.; Cheng, Z. G.; Wang, Y. B.; Li, Z. J.; Wang, C. X.; Li, Y. B.; Fang, Y. Self-Assembled 1-Octadecanethiol Monolayers on Graphene for Mercury Detection. *Nano Lett.* **2010**, *10*, 4738−4741.

(26) Li, M.; Zhou, X. J.; Ding, W. Q.; Guo, S. W.; Wu, N. Q. Fluorescent Aptamer-Functionalized Graphene Oxide Biosensor for Label-Free Detection of Mercury(II). *Biosens. Bioelectron* **2013**, *41*, 889−893.

(27) Kong, L. T.; Wang, J.; Zheng, G. C.; Liu, J. H. A Highly Sensitive Protocol (FRET/SIMNSEF) for the Determination of Mercury ions: A Unity of Fluorescence Quenching of Graphene and Enhancement of Nanogold. *Chem. Commun.* **2011**, *47*, 10389−10391.

(28) Ding, X. F.; Kong, L. T.; Wang, J.; Fang, F.; Li, D. D.; Liu, J. H. Highly Sensitive SERS Detection of Hg^{2+} Ions in Aqueous Media Using Gold Nanoparticles/Graphene Heterojunctions. *ACS Appl. Mater. Interfaces* **2013**, *5*, 7072−7078.

(29) Choi, H.; Hwang, S.; Bae, H.; Kim, S.; Kim, H.; Jeon, M. Electrophoretic Graphene for Transparent Counter Electrodes in Dye-Sensitised Solar Cells. *Electron. Lett.* **2011**, *47*, 281−283.

(30) Fan, A. P.; Ling, Y.; Lau, C. W.; Lu, J. Z. Direct Colorimetric Visualization of Mercury (Hg^{2+}) Based on the Formation of Gold Nanoparticles. *Talanta* **2010**, *82*, 687−692.

(31) Cheng, X. H.; Li, S.; Jia, H. Z.; Zhong, A. S.; Zhong, C.; Feng, J.; Qin, J. G.; Li, Z. Fluorescent and Colorimetric Probes for Mercury(II): Tunable Structures of Electron Donor and p-Conjugated Bridge. *Chem.—Eur. J.* **2012**, *18*, 1691−1699.

(32) Li, D.; Muller, M. B.; Gilje, S.; Kaner, R. B.; Wallace, G. G. Processable Aqueous Dispersions of Graphene Nanosheets. *Nat. Nanotechnol.* **2008**, *3*, 101−105.
(33) Zhao, L. F.; Li, S. J.; He, J.; Tian, G. H.; Wei, Q.; Li, H. Enzyme-Free Electrochemical Immunosensor Configured with Au-Pd Nanocrystals and N-Doped Graphene Sheets for Sensitive Detection of AFP. *Biosens. Bioelectron.* **2013**, *49*, 222−225.
(34) Zan, X. L.; Fang, Z.; Wu, J.; Xiao, F.; Huo, F. W.; Duan, H. W. Freestanding Graphene Paper Decorated with 2D-Assembly of Au@Pt Nanoparticles as Flexible Biosensors to Monitor Live Cell Secretion of Nitric Oxide. *Biosens. Bioelectron.* **2013**, *49*, 71−78.
(35) Iliut, M.; Leordean, C.; Canpean, V.; Teodorescu, C. M.; Astilean, S. A New Green, Ascorbic Acid-Assisted Method for Versatile Synthesis of Au-Graphene Hybrids as Efficient Surface-Enhanced Raman Scattering Platforms. *J. Mater. Chem. C* **2013**, *1*, 4094−4104.
(36) He, H. K.; Gao, C. Graphene Nanosheets Decorated with Pd, Pt, Au, and Ag Nanoparticles: Synthesis, Characterization, and Catalysis Applications. *Sci. China Chem.* **2011**, *54*, 397−404.
(37) Amft, M.; Lebegue, S.; Eriksson, O.; Skorodumova, N. V. Adsorption of Cu, Ag, and Au Atoms on Graphene Including van der Waals Interactions. *J. Phys.: Condens. Matter* **2011**, *23*, 395001.
(38) Xu, Z. X.; Gao, H. Y.; Guoxin, H. Solution-Based Synthesis and Characterization of a Silver Nanoparticle-Graphene Hybrid Film. *Carbon* **2011**, *49*, 4731−4738.
(39) Jin, M. H.; Kim, T. H.; Lim, S. C.; Duong, D. L.; Shin, H. J.; Jo, Y. W.; Jeong, H. K.; Chang, J.; Xie, S. S.; Lee, Y. H. Facile Physical Route to Highly Crystalline Graphene. *Adv. Funct. Mater.* **2011**, *21*, 3496−3501.
(40) Han, Y. J.; Luo, Z. M.; Yuwen, L. H.; Tian, J.; Zhu, X. R.; Wang, L. H. Synthesis of Silver Nanoparticles on Reduced Graphene Oxide under Microwave Irradiation with Starch as an Ideal Reductant and Stabilizer. *Appl. Surf. Sci.* **2013**, *266*, 188−193.
(41) Yan, Z. Q.; Xu, H. Y.; Guang, S. Y.; Zhao, X.; Fan, W. L.; Liu, X. Y. A Convenient Organic−Inorganic Hybrid Approach Toward Highly Stable Squaraine Dyes with Reduced H-Aggregation. *Adv. Funct. Mater.* **2012**, *22*, 345−352.
(42) Sun, X. H.; Li, C. P.; Wong, W. K.; Wong, N. B.; Lee, C. S.; Lee, S. T.; Teo, B. K. Formation of Silicon Carbide Nanotubes and Nanowires via Reaction of Silicon (from Disproportionation of Silicon Monoxide) with Carbon Nanotubes. *J. Am. Chem. Soc.* **2002**, *124*, 14464−14471.
(43) Abel, K. A.; Boyer, J. C.; Andrei, C. M.; van Veggel, F. C. J. M. Analysis of the Shell Thickness Distribution on NaYF4/NaGdF4 Core/Shell Nanocrystals by EELS and EDS. *J. Phys. Chem. Lett.* **2011**, *2*, 185−189.
(44) Zhang, L. B.; Tao, L.; Li, B. L.; Jing, L.; Wang, E. K. Carbon Nanotube-DNA Hybrid Fluorescent Sensor for Sensitive and Selective Detection of Mercury(II) Ion. *Chem. Commun.* **2010**, *46*, 1476−1478.